Title
Stress and earthquakes in southern California, 1850-2004

Journal
Journal of Geophysical Research-Solid Earth, 110(B5)

ISSN
0148-0227

Authors
Kagan, Yan Y
Jackson, D D
Liu, Z

Publication Date
2005-04-01

DOI
10.1029/2004JB003313

Peer reviewed

JOURNAL OF GEOPHYSICAL RESEARCH, VOL. ???, XXXX, DOI:10.1029/,

PostScript file created: January 20, 2005

Stress and earthquakes in southern California, 1850-2004

Yan Y. Kagan[1], David D. Jackson[1], and Zhen Liu[1]

[1] Department of Earth and Space Sciences, University of California, Los Angeles, California, USA

Abstract. We compute the stress tensor in the upper crust of southern California as a function of time and compare observed seismicity with the estimated stress at the time of each earthquake. Several recent developments make it possible to do this much more realistically than before: (1) a wealth of new geodetic and geologic data for southern California and (2) a catalog of moment tensors for all earthquakes with magnitudes larger than 6 since 1850 and larger than 5 since 1910. We model crustal deformation using both updated geodetic data, and geologically determined fault slip rates. We subdivide the crust into elastic blocks, delineated by faults which move freely at a constant rate below a locking depth with a rate determined by the relative block motion. We compute normal and shear stresses on nodal planes for each earthquake in the catalog. We consider stress increments from previous earthquakes ("seismic stress"), and aseismic tectonic stress, both separately and in combination. The locations and mechanisms of earthquakes are best correlated with the aseismic shear stress. Including the cumulative coseismic effects from past earthquakes does not significantly improve the correlation. Correlations between normal stress and earthquakes are always very sensitive to the start date of the catalog, whether we exclude earthquakes very close to others, and whether we evaluate stress at the hypocenter or throughout the rupture surface of an earthquake. Although the correlation of tectonic stress with earthquake triggering is robust, other results are unstable apparently because the catalog has so few earthquakes.

INDEX TERMS: Seismology (ESE): 7215 Earthquake parameters; 7209 Earthquake dynamics and mechanics; 7230 Seismicity and seismotectonics; 7230 Seismicity and seismotectonics

KEYWORDS: Stress patterns, earthquake stress triggering, normal and shear stress distributions, tectonic deformation in southern California

1. Introduction

The state of stress is considered a most important parameter for controlling the occurrence of earthquakes. Recently there has been interest in statistical analysis of stress patterns and their relations to earthquakes [*Saucier et al.*, 1992; *Reasenberg and Simpson*, 1992; *Kagan*, 1994a; *Gross and Kisslinger*, 1994; *King et al.*, 1994; *Stein et al.*, 1994; *Harris et al.*, 1995; *Harris and Simpson*, 1996; *Jaumé and Sykes*, 1996; *Stein et al.*, 1997; *Deng and Sykes*, 1997a;b *Stein*, 1999; *Ziv and Rubin*, 2000; *Parsons et al.*, 2000; *Parsons*, 2002; *Huc and Main*, 2003; *Lin and Stein*, 2004; *Steacy et al.*, 2004; *Hardebeck*, 2004; *Pollitz et al.*, 2004; *Helmstetter et al.*, 2005]; see also a review by *Harris* [1998]. Many of the stress investigations are concentrated in California. This is due to the accessibility of California earthquake faults to direct geologic study, including the measurement of fault slip rates and paleoseismic investigations of large past earthquakes. Geodetic measurements of surface strain have been available since the middle of the 19th century. A recently installed dense network of GPS stations allows for detailed mapping of tectonic deformation in California [*Shen et al.*, 1996; *Jackson et al.*, 1997]. Moreover, the first local seismographic network installed in southern California continues operation [*Hileman et al.*, 1973]. Thus, California offers a unique opportunity to study the relationship between stress and earthquakes using geologic, geodetic, and seismological data.

0148-0227/05/$9.00

Most publications above investigate stress triggering for sequences of moderate and small earthquakes. But tectonic loading due to lithospheric plate motion and its release by earthquakes have not been fully studied. The short-term influence of stress perturbations caused by earthquakes is obvious: aftershocks are usually explained by such influence. The above references strongly delineate intermediate-term stress triggering of earthquakes by recent events. However, on time scales of decades and possibly even years, tectonic stress loading will play a major role in earthquake occurrence.

Despite such long and intense study, there are still some difficulties in understanding the interaction of stresses and earthquakes in California. Its stress environment was strongly influenced by great earthquakes (with magnitude $M \geq 7.75$). For two such quakes, the 1857 Fort Tejon and 1906 San Francisco events, we have sufficient data on the slip pattern and earthquake occurrence before and after. One can conjecture that previous great quakes shaped the California stress environment to a large degree, but unfortunately we have only incomplete information on these pre-historic events from paleoseismic investigations (see, for example, *Weldon et al.* [2002], and references therein). In effect this means that we are able to study only one or two events that modified regional stress, since in general each earthquake exhibits significant random fluctuations. One cannot be sure that patterns shown by these great earthquake sequences would be applicable to other global events, or to future quakes in California.

Another problem we have to address is the influence of small earthquakes on stress. *Helmstetter et al.* [2005] argue that since earthquakes are spatially clustered, the combined influence of small earthquakes is similar to that of large

events. The degree of spatial clustering can be measured by the correlation dimension [*Kagan and Knopoff*, 1980] for earthquake hypocenters. If the correlation dimension is equal to 2, the influence of small earthquakes within a unit magnitude band approximately equals that of large earthquakes in a similar band [*Helmstetter et al.*, 2005]. Similarly, *Hanks* [1992] argues that for planar faults small earthquakes are just as important to redistribute tectonic forces as larger ones. However, if the accuracy of earthquake hypocenters is low, the correlation dimension estimate increases to about 3.0 for distances comparable to location error [*Kagan*, 1994b]. If this distance is larger than the size of the earthquake focal region, large earthquakes would appear to dominate the stress pattern. Therefore, even if small events are important in estimating the stress-earthquake relation, available data do not permit a meaningful investigation.

2. Data

Fig. 1 displays focal mechanisms for the earthquakes in southern California between 1800-2003. As the initial dataset we use historical and instrumental earthquake catalogs by the *Ellsworth* [1990] and *Toppozada et al.* [2000] . Our catalog covers the years 1800-2003, and an area defined by $32.0 - 37.0°$N and $114.0 - 122.0°$W. We added (1) recent earthquakes from the Harvard catalog [*Ekström et al.*, 2003], (2) the focal mechanism solutions and spatially distributed seismic moment from other available publications [*Båth and Richter*, 1958; *Fehler and Johnson*, 1989; *Heaton*, 1982; *Helmberger et al.*, 1992; *Hileman et al.*, 1973; *Hill et al.*, 1990; *Hutton and Jones*, 1993; *Stein and Thatcher*, 1981; *Stein and Ekström*, 1992; *Toppozada et al.*, 1986; Wesnousky, 1986; *Toppozada et al.* 2000; *Pasyanos et al.* 1996], and (3) distributed moment tensors inferred from the fault trace information [*Jennings*, 1985; 1992] and slip distribution [*Bateman*, 1961; *Sieh*, 1978] for the largest earthquakes in the 19th century.

We included all known earthquakes with $M \geq 5.0$ and represent any earthquake with $M \geq 6.5$ as an ensemble of rectangular dislocations. We also added to the Ellsworth and Toppozada et al. catalog information on the rupture pattern of the southern part of the 1906 earthquake (from *Thatcher et al.* [1997]) and the 1812 earthquake (from *Deng and Sykes* [1997a]) to create a catalog starting from 1800. We include earthquakes $6.0 \geq M \geq 5.0$ in the last 65 years from *Deng and Sykes* [1997b] as well as from other sources [*Stein and Hanks*, 1998]. For many of these ($6.0 \geq M \geq 5.0$) earthquakes, the focal mechanism is unknown; we estimated their mechanisms using a weighted average from nearby earthquakes with known focal mechanisms. In almost all cases, these quakes are large events ($M \geq 6.5$) for which either their fault traces are known, or the fault plane is delineated by aftershock pattern and surface deformation measurements. Hence, by comparing focal mechanism solutions to rupture patterns of large earthquakes, for practically all moderate and small earthquakes we could guess the fault plane and resolve the fault plane ambiguity. This catalog is called the Ellsworth/Toppozada catalog below. The catalog is available on line; the URL is http://moho.ess.ucla.edu/~kagan/cal_fps2d.dat.

Stein and Hanks [1998] argue that due to the low population level in southern California during most of the second half of the 19th century the catalog may be incomplete for earthquakes $M \leq 6.5$. However, numerical experiments show that adding and subtracting even a few in the range $6.0 \leq M \leq 6.5$ during the time period 1850-1900 would not affect the results very much.

In Fig. 1 the extended sources are thinned out for clarity; otherwise the picture would be overloaded. In the full dataset (the Ellsworth/Toppozada catalog) there are 381 "sources," including point sources for smaller earthquakes and subdivision of $M \geq 6.5$ earthquakes. For the 'thinned' catalog only 167 double-couples are displayed in the diagram. Fig. 1 shows that earthquakes are not concentrated on a few faults and the mechanisms of neighboring events may have very different orientations. Even in a neighborhood of major faults, some focal mechanisms significantly disagree with fault surface traces. This mismatch confirms the idea that major faults do not fully represent the deformation pattern, even in a region with relatively simple and well-studied tectonics. The thinned catalog also is available on line; the URL is http://moho.ess.ucla.edu/~kagan/cal_fps3a.dat.

Several other catalogs of fault-plane solutions are used in this study: the list of southern California earthquakes 1968-1993 by *Harris et al.* [1995], L. Jones' (private communication, 1993) catalog of earthquakes 1986-1993, and the list of 1990-1995 moment-tensor inversions of Terrascope records [*Thio and Kanamori*, 1995; 1996; *Zhu and Helmberger*, 1996], the University of California, Berkeley (UCB-MT) catalog [see *Pasyanos et al.*, 1996; *Tajima et al.*, 2002]. Several solutions for one earthquake are sometimes presented in the last catalog. We use the solutions based on surface waves (called UCB-MT1), and another set of solutions, derived from a three-component inversion (UCB-MT2). For the CalTech (CIT-FM) 1975-1999 catalog, E. Hauksson (personal communication, 2001) supplied a revised dataset for earthquakes with magnitude $M \geq 4.9$ [*Hardebeck and Hauksson*, 2001; *Hauksson*, 2000]. Hardebeck's 1981-2000 catalog [*Hardebeck*, 2003, private communication, see also *Hardebeck and Shearer*, 2002], based on a new method for determining first-motion focal mechanisms, was also used. *Kagan* [2002] describes the accuracy of focal mechanism evaluation for most of the above-mentioned catalogs.

3. Stress calculations

3.1. Tectonic stress calculations

We derived a theoretical estimate of the stress rate tensor at each point by (1) estimating the vector displacement rate from a "back-slip" deformation model, (2) estimating the strain rate tensor from a spatial derivative of the displacement rate, and (3) estimating the stress rate by applying Hooke's law to the strain rate. The method is described by *Ge* [1997].

The deformation model was constructed to explain the observed fault slip rates and geodetically observed velocities in southern California. In the model, the earth's crust is made up of blocks bounded by faults. Several other California block models have been proposed (e.g., *Matsu'ura et al.* [1986]; *Cheng et al.* [1987]; *Bird and Kong* [1994]; *Ward* [1996], and many others). Other applications of the back-slip model are described by *Dragert et al.* [1994], *Hashimoto and Jackson* [1993], *Henry et al.* [2001], *Mazzoti et al.* [2000].

We begin by subdividing the study area into a few dozen blocks, bounded by the major faults. We treat the tectonic motion of any point on the Earth's surface as the sum of the steady state rigid motion of its underlying block and elastic deformation of that block due to frictional forces on the block-bounding faults. Rigid block motion is computed by the plate theory of *McKenzie and Parker* [1967], in which the motion of each block is represented by a rate of rotation about an Euler pole. The rigid motion of each block is fully specified by three parameters, which could be the latitude and longitude of the Euler pole plus the rotation rate around it, or equivalently three orthogonal components of the rotation vector.

If the blocks were indeed rigid, then the theory would imply a velocity discontinuity (slip) at each block boundary. But of course the blocks are not rigid, and most faults only slip in major earthquakes. There are some exceptional

"creeping" faults that do slip continuously, although the slip rate is not necessarily equal to the rate implied by the rigid block model. To match the observed zero slip rates on faults except for the creeping ones, we assume at each point on a fault a dislocation whose slip rate equals the difference between the creep rate and the velocity discontinuity implied by the rigid block model. In most cases the creep rate is zero, and the dislocation rate is the negative of the slip rate implied by the rigid block model. The dislocation then causes elastic deformation in the block which we model using the theory of *Okada* [1992]. Assuming that deformation is indeed elastic, we can then compute the stress rate using Hooke's law. The dislocation motion can be viewed as a correction to rigid body motion and is often referred to as the "back slip" because it is in the opposite sense to that implied by rigid block motion. In practice we treat the back slip as uniform slip on rectangular fault patches. The discontinuity in rigid block motion will vary with distance along a fault, so uniform slip on a patch cannot cancel the rigid block motion at every point on the patch. However, this discrepancy can be made arbitrarily small by using small enough patches. The relative motion implied by the rigid block model will also include a normal component, because the faults cannot be everywhere parallel to the relative block motion. We treat the normal component in the same way as the tangential components: we apply a normal dislocation to cancel the rigid block motion. This allows for the equivalent of creep where there is evidence of overthrusting or basin opening on particular faults.

We assume that over geologic time earthquakes release all accumulated back-slip. Thus, the long-term slip rates on faults provide direct estimates of relative rigid block motion. Another consequence is that the back slip can also be described as a "slip deficit" to be made up over the long term by earthquake slips.

With the assumptions above, we inverted a combination of the fault slip rates and geodetic velocities estimated by the Southern California Earthquake Center (SCEC) to estimate block translation and rotation rates, from which we estimated strain rates and stress rates throughout the crust. The fault slip rates are reported in the SCEC Phase II model [*Jackson et al.*, 1995]. The geodetic data include trilateration, Global Positioning System, and Very Long Baseline Interferometry data, nearly identical to the data used to construct the SCEC version 1.0 of the SCEC crustal deformation model: http://www.data.scec.org/group_e/release.v2.

The back-slip model does have several unrealistic features, especially when the block boundaries are assumed to be "tiled" with rectangular dislocation patches. The model implies displacement discontinuities and thus stress singularities at patch boundaries. Rectangular patches can't be joined at their vertical edges unless the patches are strictly vertical. These deficiencies may be minimized by taking arbitrarily small patch size and by using the numerical calculations only in the far field (away from the patch edges). *Cohen* [1999] examines the features of the model in some detail.

3.2. Seismic stress calculations

As we indicate in Section 2, our catalog consists of two sets of earthquakes: small events ($M < 6.5$) that are represented as point sources and large earthquakes ($M \geq 6.5$). The latter events' rupture surface is divided into several (sometimes several dozen) rectangular dislocations. Depending on available information, these patches are distributed along the length of a fault and depth of a seismogenic zone.

The seismic moment M_0 can be expressed through shear elastic modulus μ, average slip u, and width and length of the rupture – W and L respectively

$$M_0 = \mu u W L\,. \qquad (1)$$

For small earthquakes we commonly used a point representation of the rupture. In other cases, assuming the ratio of rupture length to average slip $L/u = 10^4$ (we experimented with other ratio values as well), we calculate the rupture area $L \times W$ of small events using their moment value. Thereafter, by assuming their rupture depth interval, we represent them as a single rectangular dislocation. In most cases, if the depth interval is not independently known, we use 10 km for both small and large earthquakes, centered at the hypocenter. If the hypocenter depth is not known, as is common for old historical and instrumental earthquakes, we assumed it to be 10 km. For small earthquakes with a hypocenter shallower than 5 km, the calculated rupture depth interval sometimes intersects the Earth's surface; in such a case we shifted the interval down. Thus, to evaluate the stress tensor due to earthquakes we used both point representation of a seismic source as well as a rectangular model of a fault patch [*Okada*, 1992]. The shear elastic modulus value is taken as 30 GPa [*Scholz*, 2002, p. 207]. In our stress-moment correlations we compute stress at the location of the quake hypocenter for small earthquakes but at the center of the dislocation patch for large events.

4. Stress patterns and focal mechanisms of earthquakes

Fig. 2 shows the N-S component (τ_{11}) of the cumulative stress tensor for southern California due to earthquakes from 1850 to the present (January 1, 2004). At large distances, the stress distribution is dominated by the influence of several large earthquakes: the 1857 Ft. Tejon, 1872 Owens valley, 1952 Kern County, and 1992 Landers events. The seismic stress pattern forms a complex mosaic due to the interacting seismic stress fields of many earthquakes [cf. *Stein et al.*, 1992]. The complicated character of stress once again underscores the need for statistical data analysis.

Fig. 3 displays the cumulative stress change again for τ_{11} component due to tectonic deformation since 1850. The tectonic model unifies geodetic and geologic data [*Shen et al.*, 1996] (see section 3).

To compare tectonic and earthquake induced stresses, Fig. 4 shows mean-square shear stress $\bar{\tau}$ or average shear stress for the sum of seismic and tectonic stresses. The mean-square shear stress is calculated as

$$\bar{\tau} \;=\; \sqrt{2\,J_2/5}\,, \qquad (2)$$

where J_2 is the second invariant of the deviatoric stress tensor [*Jaeger and Cook*, 1979, pp. 24, 33; *Kagan*, 1994a, his Eq. 6]. The influence of tectonic stress is prevalent in the combined plot. Comparing Figures 1 and 4, we see that earthquakes occur where total (seismic + tectonic) stress is high.

We compute normal and shear stress on nodal planes for each earthquake in the catalog. We compare the focal mechanisms of quakes with the resolved shear and resolved compression before the events at their hypocenters. The fault plane determination for large ($M \geq 6.5$) earthquakes is obvious – we have a rupture model for each event. To determine which of two nodal planes is the fault plane for small earthquake, we compared their planes with the rupture direction of neighboring large earthquakes. The nodal plane more similar to large event ruptures was selected as the fault plane.

How do we correlate earthquake focal mechanisms with stress? There are significant theoretical and practical difficulties to such a comparison. First, both the focal mechanism and the stress are symmetric second-rank tensors. Focal mechanism tensors for double-couple sources have certain restrictions: their trace and determinant (i.e., the first

and third tensor invariants) are both zero. The stress tensor lacks such restrictions. Instead of the full tensorial consideration, we may calculate the normal stress σ and shear stress τ on the assumed or known earthquake fault plane. As an alternative, the tensor invariants [*Kagan*, 1994a;b] can be studied; invariants do not depend on the coordinate system in which the tensor components are represented. For example, the stress display in Fig. 4 does not depend on the coordinate system used.

Second, the component values of both stress and seismic moment tensors are heavy-tailed [*Samorodnitsky and Taqqu*, 1994; *Kagan*, 1994a;b; *Uchaikin and Zolotarev*, 1999; *Lavallée and Archuleta*, 2003; *Zaliapin et al.*, 2005]. Random variables are called "heavy-tailed" if their probability density function $\phi(x)$ has a power-law dependence for large values of the x variable

$$\phi(x) \propto x^{-1-\alpha}, \tag{3}$$

with $\alpha < 2$. For such a statistical distribution, the variance does not exist, and the mean is infinite for $\alpha < 1$. The theoretical and practical problems in handling the heavy-tailed (or stable) distributions is a rapidly developing, but still incomplete discipline in mathematical statistics [*Samorodnitsky and Taqqu*, 1994; *Uchaikin and Zolotarev*, 1999; *Zaliapin et al.*, 2005].

The collection of scalar seismic moments (M_0), proportional to the tensor norm, is well approximated by the tapered Pareto distribution (the equivalent of the modified Gutenberg-Richter law) [*Kagan and Jackson*, 2000; *Bird and Kagan*, 2004]. Components of the seismic stress tensor, calculated at the location of earthquake hypocenters, follows stable distributions [*Kagan*, 1994a;b; *Lavallée and Archuleta*, 2003] with the exponent value $\alpha \leq 1.0$. Unfortunately, as mentioned above, classical statistical tools like mathematical expectation (average), covariance, and correlation coefficient are not defined when $\alpha \leq 1.0$.

Instead of covariance, *Samorodnitsky and Taqqu* [1994, p. 103] propose for such variables the "codifference." When $\alpha = 2.0$, the stable distribution becomes the Gaussian one; for this variable the codifference equals the covariance, and the scale parameter is its standard deviation. Many obstacles arise in implementing the new techniques. As *Kagan* [1994b] pointed out, although $\alpha < 1$ for small stress values, for large values of stress, the distribution of stress components is controlled by earthquake location errors, with $\alpha \to 1$. This makes calculating the codifference problematic.

As mentioned above, the scalar seismic moment is limited for the largest earthquakes [*Kagan and Jackson*, 2000; *Bird and Kagan*, 2004]. Thus, in principle all statistical moments are finite. However, if we try to calculate the scalar moment sum

$$S = \sum M_0, \tag{4}$$

or the covariance "Cov" of the moment tensor M_{ij} with the stress tensor S_{ij}

$$\mathrm{Cov}(M_{ij}S_{ij}) = \sum_{ij} M_{ij}S_{ij}, \tag{5}$$

in both cases the sums would be completely dominated by a few largest earthquakes [*Zaliapin et al.*, 2005].

Therefore, we employ more simplified measures of tensor correlation: we normalize the tensors and look at their tensor dot-product (5) as a quantitative representation of tensor consistency. In Fig. 1 we show focal mechanisms of earthquakes colored by their consistency with combined seismic and tectonic stress (for example, see Fig. 4). To calculate the degree of correlation between the normalized seismic moment tensor m_{pq} and the normalized deviatoric stress tensor σ_{pq}, we first compute the eigenvectors of σ_{pq} and then assign the eigenvector corresponding to the largest (in absolute value) eigenvalue as the first axis. The eigenvector corresponding to the smallest (in absolute value) eigenvalue is the third axis. We normalize both tensors so they are

$$\begin{vmatrix} 1 & 0 & 0 \\ 0 & -1 & 0 \\ 0 & 0 & 0 \end{vmatrix}, \tag{6}$$

displayed in their eigenvector coordinate system, for the seismic moment of double-couple source, and

$$\begin{vmatrix} 1 & 0 & 0 \\ 0 & -A & 0 \\ 0 & 0 & A-1 \end{vmatrix} \quad \text{or} \quad \begin{vmatrix} -1 & 0 & 0 \\ 0 & A & 0 \\ 0 & 0 & 1-A \end{vmatrix}, \tag{7}$$

for the deviatoric stress tensor, where $|A-1| \leq |A| < 1$ is assumed.

Let us consider the tensor dot-product of two normalized tensors

$$P = \sum_{pq} \sigma_{pq} m_{pq}. \tag{8}$$

If m_{pq} is a normalized double-couple moment tensor as in equation 6, and σ_{pq} is a normalized deviatoric stress tensor (see equation 7), then P has the value limited between -2 and 2 [*Kagan and Knopoff*, 1985]. In (8) as opposed to Eqs (6)–(7) both tensors are represented in the same coordinate system. For $A = 1$ in (7) the P-value equals 2 if an earthquake is fully consistent with stress, and but -2 for an anti-consistent event.

Table 1 shows some average tensor dot-products (8) of stress and seismic moment $\bar{P}$ for several catalogs of focal mechanisms. We performed several tens of such calculations, with a few representative results displayed in the Table. We also show ($\sigma_{\bar{P}}$), the standard deviation of $\bar{P}$.

As a statistical test, we compare the difference between two $\bar{P}$-values with their standard deviations, $\sigma_{\bar{P}}$. For statistically independent data, the ratio

$$z = \frac{\bar{P}_1 - \bar{P}_2}{\sqrt{\sigma_1^2 + \sigma_2^2}}, \tag{9}$$

is distributed for a large number of events ($n > 30$) according to a normal (Gaussian) distribution with a standard deviation of 1. This means that if $|z| \geq 1.96$, the hypothesis of $\bar{P}$ equality can be rejected at a 95% statistical significance level.

Clearly, the components of extended earthquake sources are statistically dependent. Even if we use a point source catalog, earthquakes are clustered in space, time, and focal mechanism space [*Kagan and Jackson*, 1994]. Given the positive correlation of focal mechanisms for near-by earthquakes, the significance of small differences in z will be underestimated if we neglect the correlation. Thus, whereas large values of z indicate that $\bar{P}$-values are statistically different, small z-values may be due to data dependence.

We investigated the influence of catalog selection, catalog time and space limits, temporal delay between earthquakes (ΔT), and tectonic stress on the correlation values. Following *Harris et al.* [1995] we also tried to exclude from calculation pairs of earthquakes within a close distance in space (R) and earthquakes with a stress σ_c value below a threshold 0.001 or 0.01 MPa (0.01 or 0.1 bar). We did so because spatial concentration of hypocenters can be due to

location errors, and such earthquakes may induce spurious high stress increase. We remove in some cases earthquakes with small stress value, since it is unlikely that such stress would influence earthquake triggering.

From Table 1 we see that the low correlation between seismic stress and seismic moment strongly depends on catalog choice and parameters of calculations. In general, selecting earthquake pairs with a temporal separation of less than 500 days increases the correlation level significantly or nearly significantly for three catalogs (lines 3-5, 10-11, 17-18), and insignificantly for three catalogs (lines 7-8, 19-20, 22-23). In the last two catalogs the correlation has an opposite sign, but the $|z|$-values (9) are less than 1.96. The influence of R and σ_c on the correlation is not obvious. Comparing the first 12 lines of Table 1, we see that depending on the catalog form, correlation values may even change their sign due to random fluctuations. Random fluctuations of the $\bar{P}$-value on the order $0.2 - 0.3$ are quite common for catalogs of a few hundred or a few dozen events.

Lines 16-23 in Table 1 explore the influence of temporal delay between earthquakes [*Harris et al.*, 1995]. Contrary to *Harris et al.* [1995], we calculate the total resolved shear seismic stress due to all prior earthquakes. For *Harris et al.* [1995] catalog, the results broadly confirm their conclusions: the correlation value is significantly higher for time separation less than 1.5 years compared to longer time delays between earthquakes. However, if we use other catalogs, the results are not that clear cut: the tendency in the Ellsworth/Toppozada catalog is opposite to that in *Harris et al.* [1995], whereas there is practically no dependency of $\bar{P}$ on ΔT for Jones' (personal communication, 1993) catalog.

Lines 13-15 and 25 in Table 1 demonstrate the influence of tectonic (aseismic) stress on the correlation between the total stress prior to an earthquake and the seismic moment tensor of the event. The value of $\bar{P}$ is significantly higher when we include tectonic stress. It turns out that the result does not depend strongly on whether we use a very simple model of the tectonic stress increments (uniform N-S compression/E-W dilatation stress) or a more sophisticated one based on a block model of southern California displacement [*Ge*, 1997]. In the former case, adding the seismic to the tectonic stress degrades the correlation between the total stress and focal mechanisms of earthquakes (line 14 of Table 1).

Lines 29-33 in Table 1 show results for a few recent focal mechanism or seismic moment tensor catalogs. Only for an extensive focal mechanism catalog [*Hardebeck*, 2003, private communication] is there any positive correlation/triggering between seismic stress and earthquakes. This dependence needs to be studied in more detail.

We analyzed the influence of the Ft. Tejon 1857 earthquake on subsequent activity [*Harris and Simpson*, 1996]. Our calculations differ from those by *Harris and Simpson* [1996]: we use a larger spatial window ($32.0 - 37.0°$N, $114.0 - 122.0°$W) and another (thinned) version of the Ellsworth/Toppozada catalog. The results displayed in lines 26-28 suggest that there is no obvious 'stress shadow' in early years after the 1857 earthquake. The correlation values do not exhibit a clear pattern. *Felzer et al.* [2003] obtained a similar result.

We repeated the computations of *Harris and Simpson* [1996] using different versions of the Ellsworth/Toppozada catalog. We also added tectonic stress to the static stress from the 1857 event, making the spatial window similar to that of *Harris and Simpson* [1996] and restricting stress to values above 0.001 or 0.01 MPa (0.01 or 0.1 bar), etc. Again no obvious pattern emerges. *Stein and Hanks* [1998] suggest that the stress shadow pattern may be an artifact due to the catalog incompleteness during the second half of the 19th century.

5. Statistical distributions of stress

Figs. 5–8 display examples of the cumulative statistical distributions of stress resolved on earthquake nodal planes prior to events (prestress). To make plots more graphically clear, in the cumulative plots we assume that the first entry corresponds to all earthquakes having resolved seismic normal stress σ less than or equal to -1 MPa. Similarly, the last entry counts the normalized number of events with $\sigma \geq 1$ MPa.

Distribution of the normal stress (Fig. 5a) implies that the friction coefficient is small. According to the standard view (for instance, *Scholz* [2002]), we would expect the distribution of normal stress σ to be highly asymmetric with more earthquakes occurring when seismic stress is dilatational. Contrary to such expectations, the cumulative curves in Fig. 5a exhibit no preference for a dilatational prestress (for example, 5% of earthquakes occur when $\sigma \geq 1$ MPa – about the same number as for $\sigma \leq -1$ MPa). The curves for tectonic stress display a similar behavior; they are roughly symmetrical with regard to the point (0, 0.5).

The asymmetry of dilatational versus compressional stress would be easier to see on distribution histograms. Unfortunately, due to a relatively small number of test earthquakes, such histograms exhibit large random fluctuations, making conclusions uncertain. Hence, to better demonstrate subtle asymmetries of stress distributions, we constructed Fig. 5b and several similar diagrams which show distribution differences between negative and positive values of the normal stress. We calculate

$$[1.0 - F(-a) - F(a)], \tag{10}$$

where $F(a)$ is the value of a cumulative function corresponding to normal stress level a. If a stress distribution is symmetric with regard to the stress zero value, the above expression is zero. Let us first consider the seismic stress. The diagram shows some asymmetry: for small values of σ ($0 - 0.3$ MPa), more than 10.0% of earthquakes occur in regions of compression than in dilatational zones, i.e., contrary to the Coulomb law. A commonly accepted model suggests that the Coulomb failure stress change σ_f [*Scholz*, 2002] controls earthquake occurrence:

$$\sigma_f = \tau + \mu_f \sigma_n, \tag{11}$$

where τ is the seismic shear stress on a fault plane, μ_f is a static (positive) coefficient of friction, and σ_n is a normal stress change (positive σ_n corresponds to relative extension). For larger σ_n-values there are slightly (about 2%) more earthquakes in dilatational zones; however, for larger seismic normal stress values ($\sigma_n > 0.5$ MPa) the curve again dips close to zero. Although the curve for uniform tectonic stress implies a non-zero value for μ_f, this pattern is not reproduced in the curve corresponding to the block model. All the curves in Fig. 5b display an alternating pattern below and above zero, suggesting that their behavior may be due to random factors. The pattern for seismic and tectonic stress is again inconsistent with the idea that dilatational normal stress encourages earthquakes.

The absence, or at least, small influence of normal stress on earthquake triggering confirms the results obtained through analyzing aftershock distribution [*Kagan and Jackson*, 1998]. If the friction coefficient in the Coulomb criterion is positive, then after a strong earthquake, aftershocks and other earthquakes would concentrate in the direction of the P axis (dilatational quadrant) not the direction of the T axis (compression quadrant). Such asymmetry has not been demonstrated in analysis of global and local catalogs.

Diagrams for resolved shear stress τ (Figs. 6a and 6b) display a pattern which significantly differs from that of the normal stress. Positive τ corresponds to the stress change which has the same (consistent) sign as the seismic moment tensor of the reference earthquake. Thus, earthquakes are more likely to be induced by seismic shear stress if the stress and moment tensor of the ensuing event are coherent. There are, however, some events inconsistent with the seismic shear stress (left-hand side of Fig. 6a). In Fig. 6b the curve for seismic stress shows a weak preference for the inconsistent condition, whereas tectonic stress curves clearly testify that earthquakes are triggered by aseismic stress accumulation.

As in the previous section, we performed many other calculations of statistical distributions, modifying catalog selection and computation parameters. As another example of statistical analysis, Fig. 7 displays the difference between cumulative distributions for negative and positive values of the normal stress (as in Fig. 5b) for different time windows. Obviously the general behavior is similar to Fig. 5b. For seismic stress and for block models of tectonic stress, the values of the distribution do not display any consistent pattern: the numbers of earthquakes triggered in the dilatational volumes approximately equals the numbers in the compressional parts. Only the uniform model of tectonic stress exhibits a certain preference for dilatational triggering. With available data it is difficult to understand the causes of such behavior.

Similarly, in Fig. 8 we show the influence of shear stress triggering for the same selection of catalogs as in Fig. 7. One can draw the same conclusion from these displays as that proposed above (Fig. 6b): both tectonic stress curves support the idea that earthquakes are triggered by aseismic stress accumulation. Experimenting with various catalogs and modified assumptions shows that in most cases cumulative distributions may change by a few percent, while the major features of the distribution remain robust. The results of analyzing the statistical distributions broadly agree with the results from the previous section.

6. Discussion

Stress is believed to be the most important variable controlling triggering, earthquake occurrence, and interactions. Many interesting results have been obtained thus far (see discussion in the Introduction section and the review by *Harris* [1998]), but interpreting them in the framework of stress accumulation and release using recurrence models encounters difficulties. If a large earthquake occurs when the stress exceeds the strength of rocks, why do small earthquakes occur over the seismogenic zone all the time? If the stress value is close to the critical level over a large area, should strong earthquakes occur more frequently than usual, leading to a smaller b-value in the region? This feature has not been observed unambiguously. Or does the increased stress level simply trigger more earthquakes without regard to size? The magnitude-frequency relation for aftershocks does not seem to vary from that for all earthquakes. Does the local stress at the hypocenter control an earthquake or does regional stress over the rupture zone? What stops the progression of earthquake rupture?

If there is a stress shadow after a large earthquake in the focal zone and nearby, how can one explain aftershocks? There is no clear spatial, temporal, or magnitude boundary between the aftershocks and other earthquakes. If the increased stress triggers earthquakes and a large earthquake releases stress, why are there more aftershocks than foreshocks? Many models of stress triggering assume that the Coulomb fracture criterion is also valid for the Earth's interior, as has been established in laboratory testing of rock specimens. However, numerous attempts to evaluate the friction coefficient in situ have been inconclusive, often suggesting that the coefficient is close to zero [*Bird and Kong*, 1994; *Kagan*, 1994a; *Harris*, 1998].

In the investigations reported here, we tried to answer some of the above questions. Statistical analysis suggests a poor reproducibility of results: insignificant changes in input data or data-handling assumptions substantially modify conclusions. Although in many cases we have been able to approximately reproduce the results of other researchers by using the same data, applying similar procedures to another set of data usually leads to different results. Both the data studied and the assumptions are arbitrary, necessitating a subjective approach to their interpretation.

Catalog incompleteness and uncertainties in earthquake source parameters limit our ability to understand the relation between seismic stress and earthquake occurrence. *Helmstetter et al.* [2005] and others have shown that earthquakes below the completeness threshold of available catalogs might affect the stress as much as those in any available catalog. Large earthquakes before the start of the catalog may also overwhelm the stress from cataloged events. Thus, incompleteness seriously limits our understanding of triggering. Our results show that source uncertainty is also a serious problem. Even if uncataloged events had no effect on the stress, the uncertainties in location, size, focal mechanism, and slip distribution of cataloged events would allow for very different interpretations of the triggering by seismic Coulomb stress. Some recently available catalogs provide much improved precision, at least for smaller events [see *Helmstetter et al.*, 2005, for a discussion]. Perhaps in the future we can assess triggering with much greater confidence.

These results suggest that the evidence for earthquake triggering by seismic stress is weak. There are, among others, two reasons for this: (1) low spatial resolution of available data, and (2) a possibility that the stress acting in a focal zone may result from many large earthquakes which occurred some time ago, and we have little, if any, information about them. This apparently weak stress influence in turn makes it difficult to study using only a few case studies. A weak signal can be easily misinterpreted or biased by using various modeling assumptions and different subsets of data. Perhaps the only way to obtain reliable results is to analyze large data sets statistically or to use earthquake datasets with significantly higher location and focal mechanism accuracy.

In the preceding paragraph we mention that the evidence for earthquake triggering by seismic stress is weak. This does not by necessarily mean that the seismic stress is inconsequential in earthquake triggering. We can only compare estimated moment tensors with estimated stress tensors, and both estimates are limited by measurement errors and the adequacy of available data.

For this work we adopted a measure of correlation between a pre-existing stress tensor and an earthquake moment tensor. This criterion differs from that used by many other investigators, who often use a simple binary score based on the sign of the stress-moment correlation. Is it possible that we obtain different results from others because of our different criterion? Examination of Table 1 shows that that is not likely. The column showing "Event Numbers (+/Total)" is essentially the traditional criterion, and it agrees well with our "Correlation." Those tests that result in a high correlation also result in a high ratio of favored to unfavored earthquake mechanisms, and the same for low correlations. Our correlation method is more robust because it is based on the size, not just the sign, of the correlation between stress and moment.

7. Conclusions

We analyzed the relationship between earthquake focal mechanisms and pre-existing stress as an index of earthquake triggering. We included in pre-existing stress tectonic (aseismic) stresses and seismic stresses (from past earthquakes), both separately and in combination. Results, given in Table 1, can be summarized as follows:

1. The most robust relationship is that earthquake focal mechanisms are consistent with the tectonic stress, whether that is estimated from a simple uniform stress model or a much more detailed model based on faults and blocks.
2. Earthquake focal mechanisms are moderately well correlated with the seismic stress from earthquakes within the previous 500 days. However, this correlation is sensitive to arbitrary choices in data selection like the start time, the maximum distance considered and the maximum stress considered. Also, adding seismic stresses does not significantly improve the correlation, compared with a model based on tectonic stresses alone.
3. There is no significant correlation between earthquake focal mechanisms and the stress left by earthquakes more than 500 days before.
4. The normal component of stress has little influence on earthquake occurrence. If Coulomb stress is important in earthquake triggering, the effective coefficient of friction must be indistinguishable from zero.
5. Our results are generally consistent with other published results when we make the same choices in data selection; when we make other reasonable choices, we often get rather different results for the effect of seismic stresses. The sensitivity to arbitrary choices is due to natural variability, or to insufficient information about the stress field and focal mechanisms, rather than differences in calculation methods.

Acknowledgments. We appreciate partial support from the National Science Foundation through grants EAR 00-01128, EAR 04-09890, from CalTrans grant 59A0363, and from the Southern California Earthquake Center (SCEC). SCEC is funded by NSF Cooperative Agreement EAR-0106924 and USGS Cooperative Agreement 02HQAG0008. The authors thanks P. Bird of UCLA for very useful discussions. The comments by the reviewer Steven Ward and an anonymous reviewer as well as by the Associate Editor Joan Gomberg have significantly improved the presentation. Kathleen Jackson edited the final version. Publication 822, SCEC.

References

Amelung, F., and G. King (1997), Large-scale tectonic deformation inferred from small earthquakes, *Nature*, *386*, 702-705.

Bateman, P. C. (1961), Willard D. Johnson and the strike-slip component of fault movement in the Owens Valley, California, earthquake of 1872, *Bull. Seismol. Soc. Amer.*, *51*, 483-493.

Båth, M., and C. F. Richter (1958), Mechanisms of the aftershocks of the Kern County, California, earthquake of 1952, *Bull. Seismol. Soc. Amer.*, *48*, 133-146.

Bird P., and X. H. Kong (1994), Computer simulations of California tectonics confirm very low strength of major faults, *Geol. Soc. Amer. Bull.*, *106*, 159-174.

Bird, P., and Y. Y. Kagan (2004), Plate-tectonic analysis of shallow seismicity: apparent boundary width, beta, corner magnitude, coupled lithosphere thickness, and coupling in seven tectonic settings, *Bull. Seismol. Soc. Amer.*, *94*(6), 2380-2399.

Cheng, A., D. D. Jackson, and M. Matsu'ura (1987), Aseismic crustal deformation in the Transverse Ranges of southern California, *Tectonophysics*, *144*, 159-180.

Cohen, S. (1999), Numerical models of crustal deformation in seismic zones, *Adv. Geophys. 41*, 133-231.

Deng, J. S., and L. R. Sykes (1997a), Evolution of the stress field in southern California and triggering of moderate-size earthquakes: A 200-year perspective, *J. Geophys. Res.*, *102*, 9859-9886.

Deng, J. S., and L. R. Sykes (1997b), Stress evolution in southern California and triggering of moderate-, small-, and micro-size earthquakes, *J. Geophys. Res.*, *102*, 24,411-24,435.

Dragert, H., R.,D. Hyndman, G. Rogers, and K. Wang (1994), Current deformation and the width of the seismogenic zone of the northern Cascadia subduction thrust, *J. Geophys. Res.*, *99*, 653-668.

Ekström, G., A. M. Dziewonski, N. N. Maternovskaya and M. Nettles (2003), Global seismicity of 2001: centroid-moment tensor solutions for 961 earthquakes, *Phys. Earth Planet. Inter. 136*(3-4), 165-185.

Ellsworth, W. L. (1990), Earthquake history, 1769-1989, in: *The San Andreas fault system, California*, ed. R. E. Wallace, Geological Survey Professional Paper; P 1515, pp. 153-187.

Fehler, M., and P. Johnson (1989), Determination of fault planes at Coalinga, California, by analysis of patterns in aftershock locations, *J. Geophys. Res.*, *94*, 7496-7506.

Felzer, K. R., R. E. Abercrombie, and E. E. Brodsky (2003), Testing the stress shadow hypothesis, *Eos Trans. AGU*, *84*(47), Fall Meet. Suppl., Abstract S31A-04.

Ge, B.-X. (1997), Ph.D. dissertation, U. California, Los Angeles.

Gross, S. J., and C. Kisslinger (1994), Stress and the spatial distribution of seismicity in the central Aleutians, *J. Geophys. Res.*, *99*, 15291-15303.

Hanks, T. C. (1992), Small earthquakes, tectonic forces, *Science*, *256*, 1430-1432.

Hardebeck, J. L. (2004), Stress triggering and earthquake probability estimates, *J. Geophys. Res.*, *109*(4), Art. No. B04310

Hardebeck, J. L., and P. M. Shearer (2002), A new method for determining first-motion focal mechanisms, *Bull. Seismol. Soc. Amer.*, *92*(6), 2264-2276.

Hardebeck, J. L., and E. Hauksson (2001), Stress orientations obtained from earthquake focal mechanisms: What are appropriate uncertainty estimates? *Bull. Seismol. Soc. Amer.*, *91*, 250-262.

Harris, R. A. (1998), Introduction to special section: Stress triggers, stress shadows, and implications for on seismic hazard, *J. Geophys. Res.*, *103*, 24,347-24,358.

Harris, R. A., and R. W. Simpson (1996), In the shadow of 1857 – the effect of the great Ft Tejon earthquake on subsequent earthquakes in southern California, *Geophys. Res. Lett.*, *23*, 229-232.

Harris, R. A., R. W. Simpson, and P. A. Reasenberg (1995), Influence of static stress changes on earthquake locations in southern California, *Nature*, *375*, 221-224.

Hashimoto, M., and D. Jackson (1993), Plate tectonics and crustal deformation around the Japanese Islands, *J. Geophys. Res.*, *98*, 16,149-16,166.

Henry, P., S. Mazzotti, X. Le Pichon (2001), Transient and permanent deformation of central Japan estimated by GPS. Interseismic loading and subduction kinematics, *Earth and Planetary Science Letters*, *184*, 443-453.

Hauksson, E. (2000), Crustal structure and seismicity distribution adjacent to the Pacific and North America plate boundary in southern California, *J. Geophys. Res.*, *105*, 13,875-13,903.

Heaton, T. H. (1982), The 1971 San Fernando earthquake: a double event?, *Bull. Seismol. Soc. Am.*, *72*, 2037-2062.

Helmberger, D. V., P. G. Somerville, and E. Garnero (1992), The location and source parameters of the Lompoc, California, earthquake of 4 November 1927, *Bull. Seismol. Soc. Am.*, *82*, 1678-1709.

Helmstetter, A., Y. Y. Kagan, and D. D. Jackson (2005), Importance of small earthquakes for stress transfers and earthquake triggering, JGR, this issue, accepted http://arXiv.org/abs/physics/0407018 .

Hileman, J. A., C. R. Allen, and J. M. Nordquist (1973), *Seismicity of the Southern California Region, 1 January 1932 to 31 December 1972*, Cal. Inst. Technology, Pasadena.

Hill, D. P., J. P. Eaton, and L. M. Jones (1990), Seismicity 1980-86, in: *The San Andreas fault system, California*, ed. R. E. Wallace, Geological Survey Professional Paper; P 1515, pp. 115-151.

Huc, M., and I. G. Main (2003), Anomalous stress diffusion in earthquake triggering: Correlation length, time dependence, and directionality, *J. Geophys. Res.*, *108*(B7), ESE-1, pp. 1-12, art. no. 2324.

Hutton, L. K., and L. M. Jones (1993), Local magnitudes and apparent variations in seismicity rates in southern California, *Bull. Seismol. Soc. Am.*, *83*, 313-329.

Jackson, D. D., Aki, K., Cornell, C. A., Dieterich, J. H., Henyey, T. L., Mahdyiar, M., Schwartz, D., Ward, S. N (1995), (Working group on the probabilities of future large earthquakes in southern California), Seismic hazards in southern California: Probable earthquakes 1994-2024, *Bull. Seism. Soc. Am.*, *85*, 379-439.

Jackson, D. D., Shen, Z.-K., D. Potter, B.-X. Ge, and L.-Y. Sung (1997), Southern California deformation, *Science*, *277*, 1621-1622.

Jaeger, J. C., and N. G. W. Cook (1979), *Fundamentals of Rock Mechanics*, 3-rd ed., Chapman and Hall, London, 593 pp.

Jaumé, S. C., and Sykes, L. R. (1996), Evolution of moderate seismicity in the San Francisco Bay region, 1850 to 1993: seismicity changes related to the occurrence of large and great earthquakes, *J. Geophys. Res.*, *101*, 765-789.

Jennings, C. W. (1985), An explanatory text to accompany the 1:750,000 scale fault and geologic maps of California, *Bulletin – California, Division of Mines and Geology*, *201* (197 pp.

Jennings, C. W. (1992), Preliminary fault activity map of California, Sacramento, Calif., California Div. Mines and Geology Open-File report 92-03.

Kagan, Y. Y. (1994a), Incremental stress and earthquakes, *Geophys. J. Int.*, *117*, 345-364.

Kagan, Y. Y. (1994b), Distribution of seismic static stress caused by earthquakes, *Nonlinear Processes Geophys.*, *1*, 172-181.

Kagan, Y. Y. (2002), Modern California earthquake catalogs and their comparison, *Seism. Res. Lett.*, *73*(6), 921-929.

Kagan, Y. Y., and D. D. Jackson (1994), Long-term probabilistic forecasting of earthquakes, *J. Geophys. Res.*, *99*, 13,685-13,700.

Kagan, Y. Y., and D. D. Jackson (1998), Spatial aftershock distribution: Effect of normal stress, *J. Geophys. Res.*, *103*, 24,453-24,467.

Kagan, Y. Y., and D. D. Jackson (2000), Probabilistic forecasting of earthquakes, *Geophys. J. Int.*, *143*, 438-453.

Kagan, Y. Y., and L. Knopoff (1980), Spatial distribution of earthquakes: The two-point correlation function, *Geophys. J. Roy. astr. Soc.*, *62*, 303-320.

Kagan, Y. Y., and L. Knopoff (1985), The two-point correlation function of the seismic moment tensor, *Geophys. J. R. astr. Soc.*, *83*, 637-656.

King, G. C. P., Stein, R. S., and J. Lin (1994), Static stress changes and the triggering of earthquakes, *Bull. Seismol. Soc. Amer.*, *84*, 935-953.

Lavallée, D., and R. J. Archuleta (2003), Stochastic modeling of slip spatial complexities for the 1979 Imperial Valley, California, earthquake, *Geophys. Res. Lett.*, *30*(5), Art. No. 1245.

Lin, J., and R. S. Stein (2004), Stress triggering in thrust and subduction earthquakes and stress interaction between the southern San Andreas and nearby thrust and strike-slip faults, *J. Geophys. Res.*, *109*B2, Art. No. B02303.

Matsu'ura, M., D. D. Jackson, and A. Cheng (1986), Dislocation model for aseismic crustal deformation at Hollister, California, *J. Geophys. Res.*, *91*, 12,661-12,674.

Mazzotti, S., X. LePichon, P. Henry, S. Miyazaki (2000), Full interseismic locking of the Nankai and Japan- West Kurile subduction zones: an analysis of uniform elastic strain accumulation in Japan constrained by permanent GPS, *J. Geophys. Res.*, *105*, 13,159-13,177.

McKenzie, D., and R. L. Parker (1967), The North Pacific: an example of tectonics on a sphere, *Nature*, *216*, 1276-1280.

Okada, Y. (1992), Internal deformation due to shear and tensile faults in a half-space, *Bull. Seismol. Soc. Amer.*, *82*, 1018-1040.

Parsons, T. (2002), Global Omori law decay of triggered earthquakes: Large aftershocks outside the classical aftershock zone, *J. Geophys. Res.*, *107*, 2199, doi:10.1029/2001JB000646.

Parsons, T., S. Toda, R. S. Stein, A. Barka, and J. H. Dieterich (2000), Heightened odds of large earthquakes near Istanbul: An interaction-based probability calculation, *Science*, *288*, 661-665

Pasyanos, M. E., D. S. Dreger, and B. Romanowicz (1996), Toward real-time estimation of regional moment tensors, *Bull. Seismol. Soc. Amer.*, *86*, 1255-1269.

Pollitz, F., W. H. Bakun, and M. Nyst (2004), A physical model for strain accumulation in the San Francisco Bay region: Stress evolution since 1838, *J. Geophys. Res.*, *109*B11, B11408, 10.1029/2004JB003003

Reasenberg, P. A, and Simpson R. W. (1992), Response of regional seismicity to the static stress change produced by the Loma-Prieta earthquake, *Science*, *255*, 1687-1690.

Samorodnitsky, G., and M. S. Taqqu (1994), *Stable non-Gaussian Random Processes: Stochastic Models with Infinite Variance*, New York, Chapman & Hall, 632 pp.

Saucier, F., E. Humphreys, and R. Weldon (1992), Stress near geometrically complex strike-slip faults – application to the San Andreas fault at Cajon pass, southern California, *J. Geophys. Res.*, *97*, 5081-5094.

Scholz, C. H. (1998), Earthquakes and friction laws, *Nature*, *391*, 37-42.

Scholz, C. H. (2002), *The Mechanics of Earthquakes and Faulting*, Cambr. Univ. Press, Cambridge, 2nd ed., pp. 471.

Shen, Z.-K., D. D. Jackson, and B. X. Ge (1996), Crustal deformation across and beyond the Los Angeles basin from geodetic measurements, *J. Geophys. Res.*, *101*, 27,957-27,980.

Sieh, K. E. (1978), Slip along the San Andreas Fault associated with the great 1857 earthquake, *Bull. Seismol. Soc. Am.*, *68*, 1421-1447.

Steacy, S., D. Marsan, S. S. Nalbant, and J. McCloskey (2004), Sensitivity of static stress calculations to the earthquake slip distribution, *J. Geophys. Res.*, *109*(B4), Art. No. B04303.

Stein, R. S. (1999), The role of stress transfer in earthquake occurrence, *Nature*, *402*, 605-609.

Stein, R. S., Barka, A. A., and Dieterich, J. H. (1997), Progressive failure on the North Anatolian fault since 1939 by earthquake stress triggering, *Geophys. J. Int.*, *128*, 594-604.

Stein, R. S., and G. Ekström (1992), Seismicity and geometry of a 110-km-long blind thrust fault; 2, Synthesis of the 1982-1985 California earthquake sequence, *J. Geophys. Res.*, *97*, 4865-4883.

Stein, R. S., and T. C. Hanks (1998), $M \geq 6$ earthquakes in southern California during the twentieth century: no evidence for a seismicity or moment deficit, *Bull. Seismol. Soc. Amer.*, *88*, 635-652.

Stein, R. S., G. C. P. King, and J. Lin (1994), Stress triggering of the 1994 $M = 6.7$ Northridge, California, earthquake by its predecessors, *Science*, *265*, 1432-1435.

Stein, R. S., and W. Thatcher (1981), Seismic and aseismic deformation associated with the 1952 Kern County, California, earthquake and relationship to the Quaternary history of the White Wolf Fault, *J. Geophys. Res.*, *86*, 4913-4928.

Tajima, F., C. Megnin, D. S. Dreger, and B. Romanowicz (2002), Feasibility of real-time broadband waveform inversion for simultaneous moment tensor and centroid location determination, *Bull. Seismol. Soc. Amer.*, *92*(2), 739-750.

Tabei, T., M. Hashimoto, S. Miyazaki, K. Hirahara, F. Kimata, T. Matsushima (2002), Subsurface structure and faulting of the Median Tectonic Line, southwest Japan inferred from GPS velocity field, *Earth Planets Space*, *54*, 1065-1070.

Thatcher, W., G. Marshall, and M. Lisowski (1997), Resolution of fault slip along 470-km-long rupture of the great 1906 San Francisco earthquake and its implications, *J. Geophys. Res.*, *102*, 5353-5367.

Thio, H. K., and H. Kanamori (1995), Moment-tensor inversions for local earthquakes using surface waves recorded at Terrascope, *Bull. Seismol. Soc. Amer.*, *85*, 1021-1038.

Thio, H. K., and H. Kanamori (1996), Source complexity of the 1994 Northridge earthquake and its relation to aftershock mechanisms, *Bull. Seismol. Soc. Amer.*, *86*, S84-S92.

Toppozada, T. R., C. R. Real, and D. L. Parke (1986), Earthquake history of California, *California Geology*, February, 27-33.

Toppozada, T., D. Branum, M. Petersen, C. Hallstrom, C. Cramer, and M. Reichle (2000), *Epicenters of and Areas Damaged by $M \geq 5$ California Earthquakes, 1800-1999*, Map sheet 49, Div. Mines Geology, California.

Uchaikin, V. V. and V. M. Zolotarev (1999), *Chance and Stability: Stable Distributions and Their Applications*, Utrecht: VSP International Science Publishers, 596 pp.

Ward, S. N. (1996), A synthetic seismicity model for southern California: Cycles, probabilities, and hazard, *J. Geophys. Res.*, *101*B10, 22,393-22,418.

Weldon, R. J., T. E. Fumal, T. J. Powers, S. K. Pezzopane, K. M. Scharer, and J. C. Hamilton (2002), Structure and earthquake offsets on the San Andreas fault at the Wrightwood, California, paleoseismic site, *Bull. Seismol. Soc. Amer.*, *92*, 2704-2725.

Wesnousky, S. G. (1986), Earthquakes, Quaternary faults, and seismic hazard in California, *J. Geophys. Res.*, *91*, 12,587-12,631.

Zaliapin, I. V., Y. Y. Kagan, and F. Schoenberg (2005), Approximating the distribution of Pareto sums, *Pure Appl. Geoph.*, accepted http://scec.ess.ucla.edu/~ykagan/zks_index.html .

Zhu, L. P., and D. V. Helmberger (1996), Advancement in source estimation techniques using broadband regional seismograms, *Bull. Seismol. Soc. Amer.*, *86*, 1634-1641.

Ziv, A., and A. M. Rubin (2000), Static stress transfer and earthquake triggering: No lower threshold in sight?, *J. Geophys. Res.*, *105*, 13631-13642.

Yan Y. Kagan, Department of Earth and Space Sciences, University of California, Los Angeles, California, 90095-1567, USA; (e-mail: ykagan@ucla.edu)

David D. Jackson, Department of Earth and Space Sciences, University of California, Los Angeles, California. (e-mail: djackson@ucla.edu)

Zhen Liu, Department of Earth and Space Sciences, University of California, Los Angeles, California. (e-mail: zliu@zephyr.ess.ucla.edu)

Table 1. Resolved stress correlation with focal mechanisms of earthquakes

No	Catalog log	Event Numbers (+/Total)	Correlation $\bar{P} \pm \sigma_{\bar{P}}$	Tectonic Stress	Time Limit ΔT (days)	Distance Limit R (km)	Stress Limit σ_c (bar)
1	a	194/380	0.15 ± 0.07	–	–	–	–
2	a	209/380	0.23 ± 0.06	–	–	> 10	–
3	a	103/144	0.44 ± 0.08	–	< 500	> 10	–
4	a	204/380	0.20 ± 0.06	–	> 500	> 10	–
5	a	150/311	0.01 ± 0.07	–	> 500	> 10	0.01
6	b	50/84	0.18 ± 0.09	–	< 500	> 10	–
7	b	86/166	0.12 ± 0.09	–	> 500	> 10	–
8	b	18/35	0.04 ± 0.12	–	< 500	> 10	0.01
9	c	56/112	-0.01 ± 0.11	–	–	–	–
10	d	366/547	0.53 ± 0.05	–	< 500	> 10	–
11	d	291/650	-0.02 ± 0.05	–	> 500	> 10	–
12	c	11/30	-0.07 ± 0.18	–	< 500	> 10	0.01
13	a	308/381	0.96 ± 0.05	U	–	–	–
14	a	334/379	1.20 ± 0.04	UN	–	–	–
15	a	309/381	1.06 ± 0.06	B	–	–	–
16	h	14/21	0.36 ± 0.24	–	–	> 5	0.1
17	h	11/14	0.65 ± 0.24	–	< 550	> 5	0.1
18	h	3/7	-0.03 ± 0.52	–	> 550	> 5	0.1

In third column '+/Total' signifies that ratio of earthquakes with positive stress-moment correlation to total event numbers is shown; in the sixth column $\Delta T < 500$, for example, means that only events within 500 days were used in calculation of earthquake induced stress.

[a] Ellsworth/Toppozada catalog with extended sources; time window 1850-1998, space window $32.0 - 37.0°$N, $114.0 - 122.0°$W;

[b] Ellsworth/Toppozada thinned catalog with extended sources;

[b1] Ellsworth/Toppozada thinned catalog with extended sources, time window 1857-1907;

[b2] Ellsworth/Toppozada thinned catalog with extended sources, time window 1908-1957;

[b3] Ellsworth/Toppozada thinned catalog with extended sources, time window 1958-1998;

[c] Ellsworth/Toppozada catalog with point sources;

[d] Deng-Ellsworth catalog with extended sources; time window 1812-1998, space window $32.0 - 37.0°$N, $114.0 - 122.0°$W;

[h] *Harris et al.* [1995] catalog;

Table 1. Continued

No	Catalog log	Event Numbers (+/Total)	Correlation $\bar{P} \pm \sigma_{\bar{P}}$	Tectonic Stress	Time Limit ΔT (days)	Distance Limit R (km)	Stress Limit σ_c (bar)
19	c1	5/13	-0.12 ± 0.29	–	< 500	> 10	0.01
20	c1	17/25	0.35 ± 0.20	–	> 500	> 10	0.01
21	j	31/49	0.24 ± 0.14	–	–	> 5	0.1
22	j	29/46	0.25 ± 0.14	–	< 550	> 5	0.1
23	j	2/3	0.30 ± 0.18	–	> 550	> 5	0.1
24	t	135/258	0.07 ± 0.06	–	–	–	–
25	t	192/258	0.55 ± 0.06	U	–	–	–
26	b1	16/27	0.34 ± 0.19	–	–	–	0.01
27	b2	27/37	0.66 ± 0.17	–	–	–	0.01
28	b3	43/78	0.28 ± 0.11	–	–	–	0.01
29	d1	15/8	0.17 ± 0.28	–	–	> 5	0.1
30	d2	9/4	0.0 ± 0.32	–	–	> 5	0.1
31	h1	24/18	0.50 ± 0.20	–	–	> 5	0.1
32	h2	234/160	0.52 ± 0.07	–	–	> 5	0.1
33	h3	700/483	0.49 ± 0.04	–	–	> 5	0.1

^{c1} Ellsworth/Toppozada catalog with point sources, time window 1968-1995, space window $32.5 - 35.2°$N, $115.0 - 120.0°$W;

^{j} Jones (1993, personal communication) catalog;

^{t} *Thio and Kanamori* [1995; 1996] and *Ellsworth* [1990] catalogs;

^{d1} Berkeley UCB-MT1 1991-1999 catalog;

^{d2} Berkeley UCB-MT2 1991-2003 catalog;

^{h1} Hauksson 1975-1999 (personal communication, 2001) catalog;

^{h2} Hardebeck 1981-2001 (personal communication, 2003) catalog, events $M \geq 3.0$;

^{h3} Hardebeck 1981-2001 (personal communication, 2003) catalog, events $M \geq 2.5$;

^{U} uniform N-S compression/E-W dilatation stress;

^{UN} uniform N-S compression/E-W dilatation stress, no seismic stress;

^{B} stress calculated using the block model.

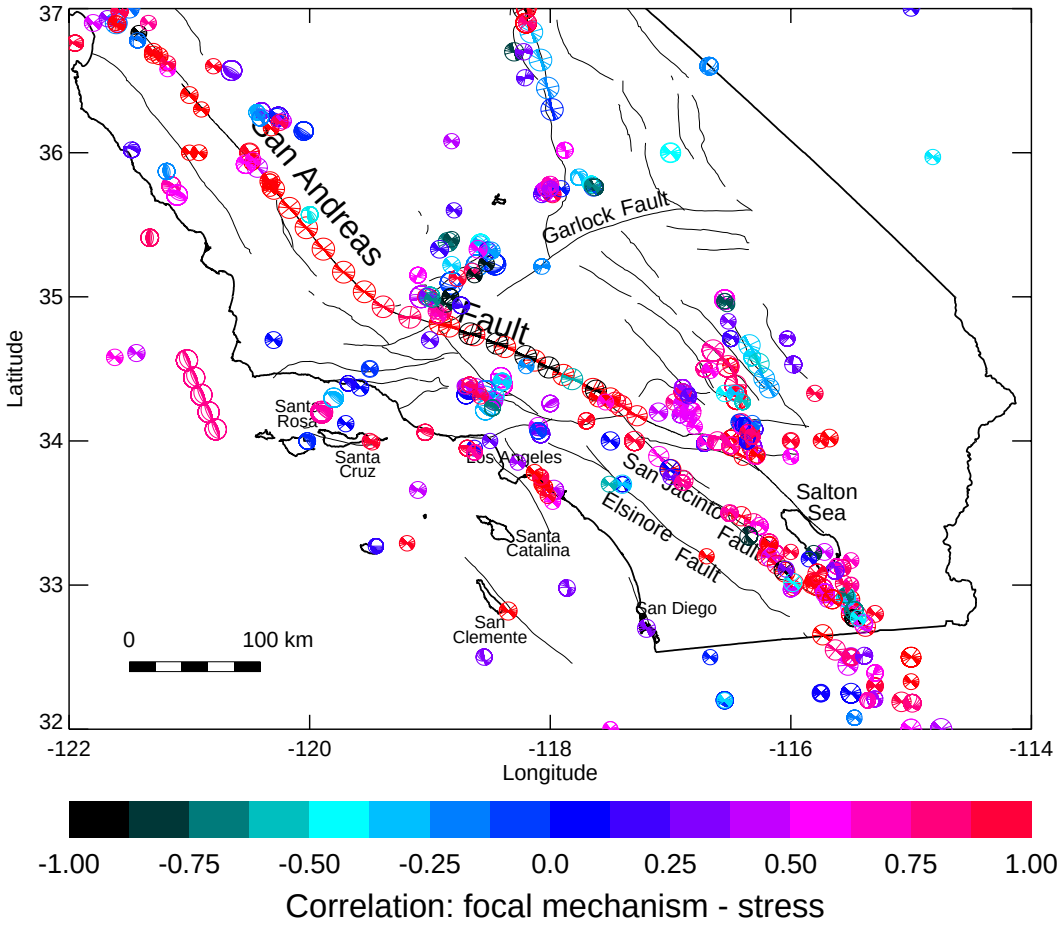

Figure 1. Focal mechanisms of earthquakes for 1850-2003 in the southern California area and major surface faults. Lower hemisphere diagrams of focal spheres are shown; the diagrams can be thought of as 3-D rotations of the mechanism. Data are from *Ellsworth* [1990] and *Toppozada et al.* [2000] with addition of others. All events with magnitude $m \geq 6.5$ are replaced by extended sources, containing several smaller rectangular dislocation patches matching total earthquake moment. Symbol size is proportional to earthquake magnitude. Since earthquake magnitude fluctuates in the diagram from 5.0 to 6.4, the symbol sizes are not very different. More densely striped 'beachballs' correspond to point sources, less densely striped symbols are used for assembled extended sources. Stripes in beachballs are concentrated towards the assumed earthquake fault-plane. Diagrams are colored according to the consistency of the focal mechanisms with the tectonic and coseismic static stress accumulated, starting with 1800, by origin time of earthquake. Red means that the focal mechanism is consistent (correlated) with the stress tensor, blue (black) signifies the anti-correlation.

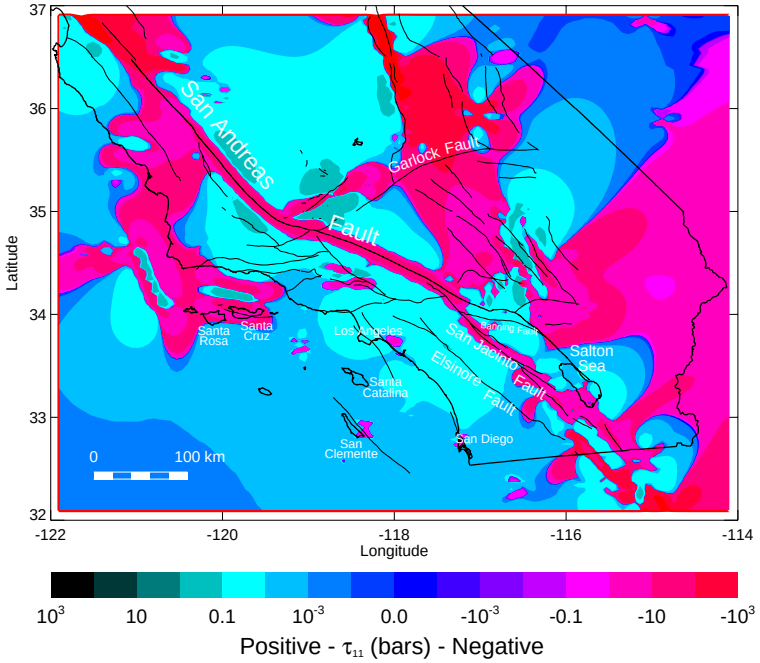

Figure 2. Earthquake induced stress in southern California at the Earth's surface. The modified Ellsworth/Toppozada catalog 1850-2004 is used. Horizontal (N-S) stress component τ_{11} is shown.

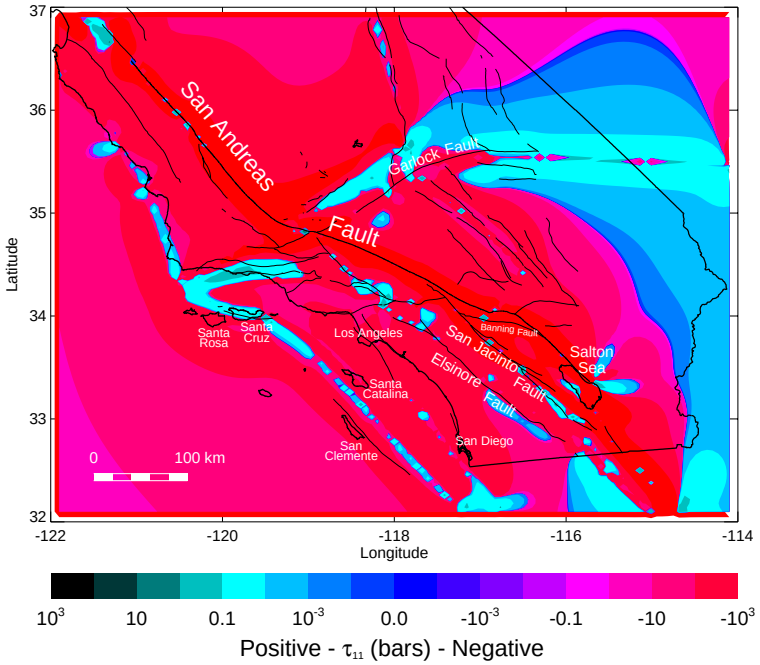

Figure 3. Cumulative tectonic stress change in southern California, since 1850, calculated using elastic blocks, delineated by faults, at the Earth's surface [*Ge*, 1997]. Horizontal (N-S) stress component τ_{11} is shown.

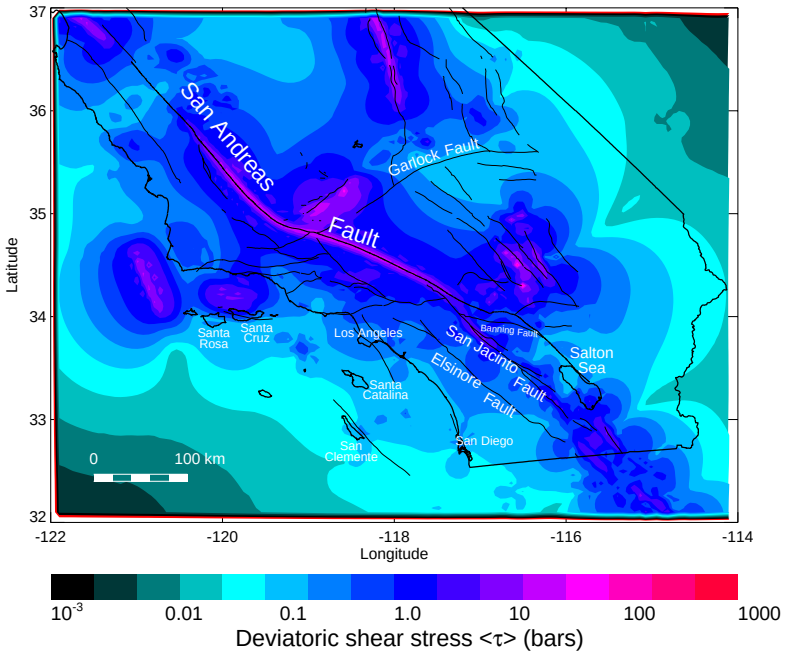

Figure 4. Shear stress in southern California at the Earth's surface. The modified Ellsworth/Toppozada catalog 1800-2004 is used. Mean-square seismic + tectonic shear stress is shown.

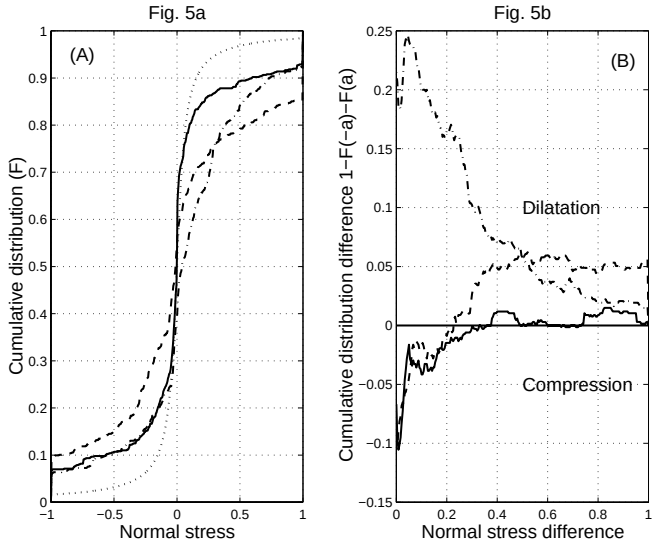

Figure 5. Statistical distributions of normal stress σ_n resolved on earthquake nodal planes prior to earthquakes in the Ellsworth/Toppozada catalog (1850-2004). In all plots, the solid line is for the seismic stress due to earthquakes, the dash-dotted line is for the seismic plus uniform tectonic stress, and the dashed line is for the seismic plus tectonic stress, according to block model of displacement. (a) Cumulative distribution for the stress normal to the fault plane. Dotted line is for the Cauchy distribution. The negative stress values correspond to compression. (b) Difference between cumulative distributions for negative and positive values of the normal stress (see Fig. 5a). Absolute value of the stress is abscissa of plot. Values above zero correspond to prevalence of dilatation over compression for resolved stress at centroids.

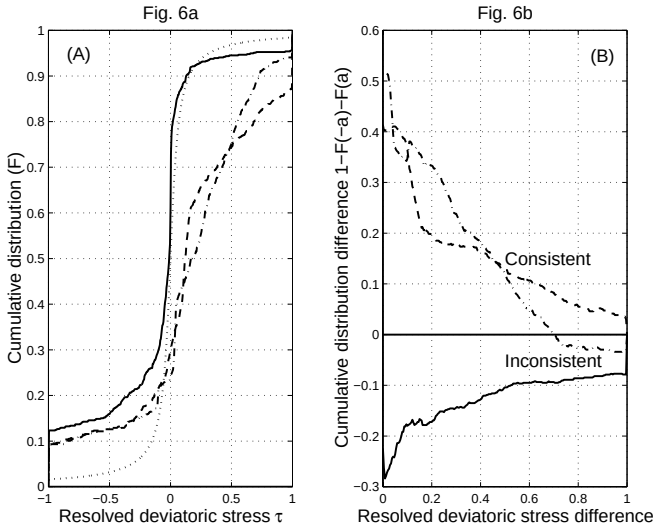

Figure 6. Statistical distributions of shear stress τ resolved on earthquake nodal planes prior to earthquakes in the Ellsworth/Toppozada catalog (1850-2004). In all plots, the solid line is for the seismic stress due to earthquakes, the dash-dotted line is for the seismic plus uniform tectonic stress, and the dashed line is for the seismic plus tectonic stress, according to block model of displacement. Plots are similar to Figs. 5a and 5b, but the resolved shear stress is plotted. (a) Resolved shear stress, the stress negative values correspond to focal mechanisms inconsistent with the stress. (b) Resolved shear stress difference, the values above zero correspond to resolved stress be consistent with a focal mechanisms at centroids.

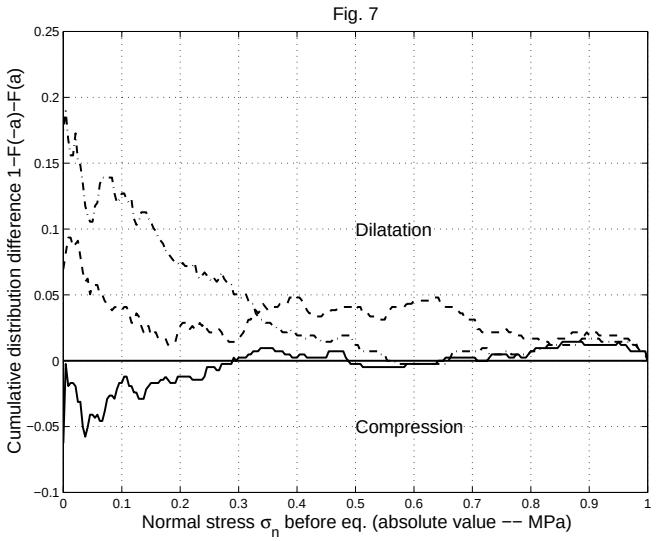

Figure 7. Difference between cumulative distributions for negative and positive values of the normal stress (compare to Fig. 5b) for the Ellsworth/Toppozada catalog (1932-2004). All lines and diagrams are similar to Fig. 5b.

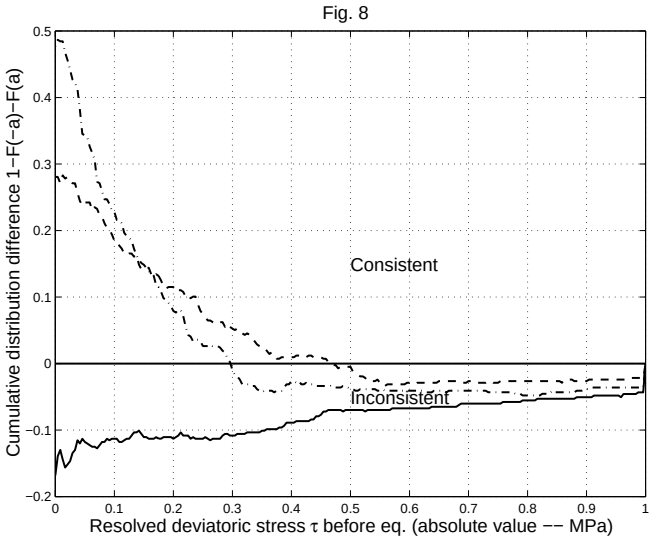

Figure 8. Similar to Fig. 7, but the resolved shear stress is plotted (compare to Fig. 6b) for the Ellsworth/Toppozada catalog (1932-2004). All lines and diagrams are similar to Fig. 6b.